Scientific Research

Measurement of the Natural Frequency and Mode Shape of Prefabricated Concrete Wind Turbine Towers via the DIC Method

Zhenwei Guo [1], Kangle Chen [2], Zhongze Sun [3,4], Lei Hong [5], Yan Xu [6] and Sihang Wei [2,*]

[1] Department of Bridge Engineering, Tongji University, Shanghai 200092, China;
[2] ZRD New Energy Solutions Co., Ltd., Shanghai 201108, China;
[3] State Key Laboratory of Intelligent Manufacturing Equipment and Technology, Huazhong University of Science and Technology, Wuhan 430074, Hubei Province, China;
[4] Dongfang Electric Wind Power Co., Ltd., Deyang 618000, Sichuan Province, China;
[5] Wuhan Sinorock Monitor&Control Technology Co., Ltd., Wuhan 430223, Hubei Province, China;
[6] Tongna Testing & Certification Group Co., Ltd., Shanghai 200331, China.
* Correspondence: weisihang@zwindtowers.com

Abstract: Resonance between wind turbine towers and rotors can severely compromise the safety of wind turbines. This study proposes a measurement method based on the digital image correlation (DIC) technique for determining the natural frequencies of prestressed concrete towers. The approach employs high-pass filtering and wavelet transform to reconstruct vibration signals, followed by the use of Welch's method to calculate the power spectrum of the reconstructed signals. The natural frequencies are identified from the spectral peaks, and the first- and second-order modes of the tower are determined through singular value decomposition (SVD). The measured first-order natural frequencies of the concrete tower under three operating conditions—turbine during stoppage, stable operation, and transition from stoppage to stable operation—are 0.2631 Hz, 0.2636 Hz, and 0.2782 Hz, respectively, whereas the second-order natural frequencies are 0.8624 Hz, 1.0397 Hz, and 0.8374 Hz, respectively. The first-order mode shapes correspond to unidirectional bending of the tower, and the second-order mode shapes correspond to reverse bending. The results demonstrate that the DIC method is an effective, convenient, and safe approach for measuring the natural frequencies of wind turbine towers, with significant practical value.

Keywords: wind turbine tower; DIC method; displacement tracking; signal processing; natural frequency; mode shape

1 Introduction

With the continuous advancement of wind power generation technology, the capacity of wind turbine installations is steadily increasing, with longer blades and taller towers being developed to accommodate these advancements [1]. Structurally, wind turbines are becoming lighter and more flexible. During operation, under the combined effects of random wind loads and periodic excitation from blade rotation, the towers are subjected to vibrations and deformations. These vibrations generate inertial forces, which not only induce additional stresses in the tower but also lead to deformations and vibrations at the rotor atop the tower, thereby affecting its structural integrity. Therefore, when designing and operating wind turbine towers, it is essential to consider the structural dynamics of the tower. Vibration analysis must be conducted to determine the natural frequencies of the tower, ensuring that it does not experience harmful or excessive vibrations, the aim of which is to prevent resonance between the rotor and the tower caused by excitations and wind loads [2].

In the design phase, the natural frequency of a wind turbine tower is determined primarily through two methods: analytical calculations and numerical simulations.

For analytical calculations, Lei et al. proposed a method for calculating the prestressed fundamental frequency of wind turbine towers on the basis of the Rayleigh method. This approach accounts for the structural form and mechanical characteristics of the tower, incorporating the prestressing effects caused by the nacelle and rotor masses on the tower [3]. For numerical calculations, Yang et al. developed a method to compute the natural frequencies of offshore wind turbine towers that considers the variable cross-sectional characteristics of the tower. The validity of this method was verified through practical engineering applications [4].

In summary, while refined finite element models can accurately determine the fundamental frequency of a wind turbine tower, the modeling process is highly complex and labor intensive, making it unsuitable for the simplified and rapid calculations required in the preliminary design phase. The current analytical methods are relatively simplistic, as they do not account for the variable stiffness characteristics of the tower cross-section or the deformations caused by the nacelle and rotor loads. Consequently, their accuracy is insufficient to meet the practical demands of engineering applications.

In the operational phase, efficiently and accurately measuring the natural frequency of a wind turbine tower remains a significant challenge. The commonly used method involves collecting vibration signals, such as acceleration, from the tower during its operation using sensors. These vibration signals are processed to generate time-domain signals, which are then transformed into frequency-domain spectra through Fourier transform. The location of the highest peak in the resulting spectrum is taken as the natural frequency of the tower. However, this method requires sensors to be placed at specific measurement points on the tower before testing. Owing to the large sizes and complex structures of wind turbine towers, practical implementation often faces challenges, such as sensor placement difficulties or insufficient measurement points.
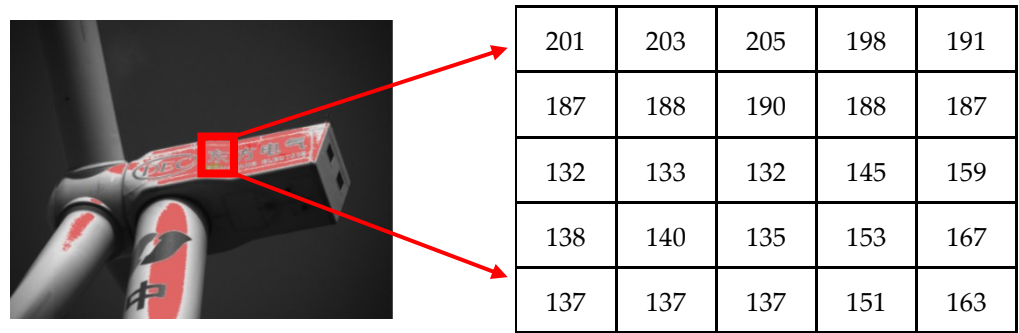
The digital image correlation (DIC) method, also known as the digital speckle correlation (DSC) method, is an image measurement technique rooted in computer vision technology. It uses the random speckle patterns naturally distributed on an object's surface or artificially applied pseudorandom speckle fields as carriers of deformation information. As a novel experimental mechanics method, the DIC method enables full-field displacement and strain analysis of material or structural surfaces under external loads or other influencing factors. This method offers several advantages, including both global and local deformation measurement capabilities, noncontact measurement, minimal site requirements, simple implementation, and wide applicability. Consequently, it has been widely used across numerous fields. In this study, the DIC method is employed to measure the natural frequencies of concrete towers, and the test results are analyzed to explore the feasibility of using the DIC method to measure the natural frequencies of wind turbine towers.

2 Basic Principles of DIC

2.1 Digital Characteristics of Images and Correlation

Images are stored in a matrix form within a computer. As shown in Figure 1, the resolution of an image corresponds to the number of rows and columns in this matrix,

and the elements of the matrix range from 0 to 255, representing the grayscale values of individual pixels.

201	203	205	198	191
187	188	190	188	187
132	133	132	145	159
138	140	135	153	167
137	137	137	151	163

Figure 1   Image storage format

In the DIC method, a fixed-view camera continuously records the displacement information of the deformation information carrier, resulting in a set of images with identical resolution. Let the grayscale matrices of the images before and after deformation be $I = I(x, y)$ and $J = J(x, y)$, respectively. The correlation C between the two images before and after deformation is defined as follows:

$$C = \frac{\sum_A I(x,y)J(x,y)}{\sum_A I^2(x,y) \cdot \sum_A J^2(x,y)} \tag{1}$$

where A represents the pixel range of the image and where x and y denote the horizontal and vertical position information of the pixels, respectively. The correlation C ranges from 0 to 1, with a larger C indicating greater similarity between two images.

2.2   Displacement Tracking

By utilizing the correlation C calculated from Equation (1), the displacement of the information carrier can be tracked. The method is as follows.

The displacements of the carrier in the image before and after deformation are defined as $(\Delta x, \Delta y)$. A reference subregion B is selected around the information carrier. The grayscale matrices of B before and after displacement are denoted as $I = I(x, y)$ and $J = J(x + \Delta x, y + \Delta y)$, respectively ($x, y \in B \in A$). Substituting these matrices into Equation (1), the correlation between the two matrices is expressed as shown in Equation (2):

$$C(\Delta x, \Delta y) = \frac{\sum_B I(x,y)J(x + \Delta x, y + \Delta y)}{\sum_B I^2(x,y) \cdot \sum_B J^2(x + \Delta x, y + \Delta y)} \tag{2}$$

During the displacement tracking process, the reference subregion B moves pixel by pixel on the deformed image until all selectable pixel points are traversed. Each time the reference subregion B moves, a displacement $(\Delta x, \Delta y)$ and the corresponding correlation coefficient C are recorded, ultimately forming a matrix $C(\Delta x, \Delta y)$. In matrix C, the $(\Delta x, \Delta y)$ of the maximum element, which indicates the highest correlation, represents the displacement of the information carrier.

Figure 2 illustrates the basic method of DIC for displacement tracking. a) shows the image of the red cross before deformation, with its grayscale matrix denoted as $I(x, y)$. In this image, an information carrier P is selected, with its initial position at $P_1(x_1, y_1)$. A reference subregion centered on P is established, and the size of the subregion and the grayscale information of the pixels within the area are recorded.

b) shows the image of the cross after displacement, with its grayscale matrix denoted as $J(x, y)$. The cross has undergone translation and rotation. The area surrounding point $P_2(x_2, y_2)$ after deformation is defined as the deformation subregion. c) is a schematic diagram of the displacement tracking process. The box formed by a solid line represents the search subregion during displacement tracking, and the areas of the three subregions are equal. The search subregion starts from $P_1(x_1, y_1)$ and moves sequentially along the x and y directions, traversing all pixel positions in J. When the search subregion overlaps with the deformed subregion, the correlation between the search subregion in J and the reference subregion in I reaches its maximum. This indicates that the displacement of the information carrier P has been successfully tracked. d) and e) are the 3D surface plot and the heatmap of matrix C, respectively.
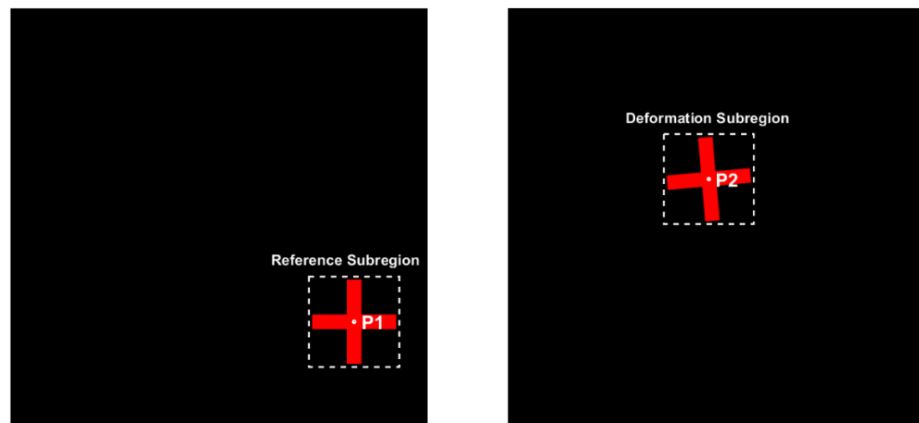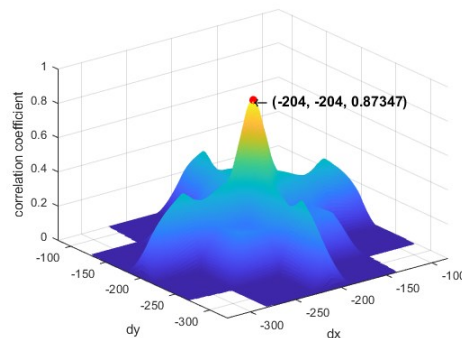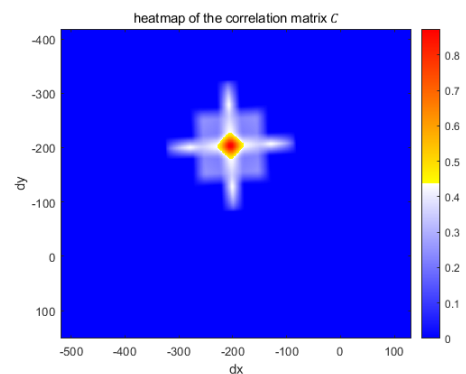

a) The cross before displacement

b) The cross after displacement
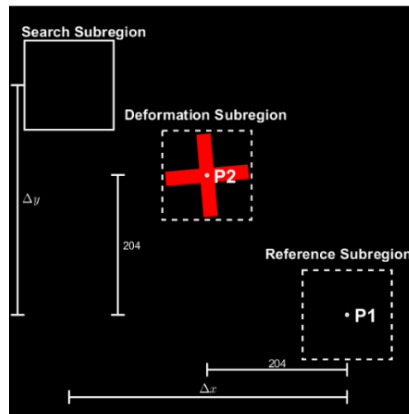
c) The displacement tracking process

d) The displacement and correlation coefficient 3D surface plot


e) The displacement and correlation coefficient heatmap

Figure 2   Basic DIC method for displacement tracking

Figure 2 shows that when $\Delta x = -204$ and $\Delta y = -204$, the correlation reaches its maximum, with $C_{\max}$, which indicates that during this deformation, the information carrier P moved 204 pixels to the left and 204 pixels upward. By repeating the above steps, the displacement of P can be continuously tracked.

2.3   DIC Search Algorithm

The essence of the DIC method is determining how many pixels at the same point on an object have been displaced between two images taken before and after deformation. Its basic concept involves dividing the search process into two parts: integer-pixel search and subpixel search [5]. Integer-pixel search is conducted in units of discrete pixels, enabling efficient localization over a large area. Subpixel search refines the integer-pixel search results, further enhancing the precision and accuracy of the displacement calculations. The operational approach to integer-pixel search can be summarized as follows: Step 1 involves an initial coarse search to identify an optimal starting point; Step 2 involves performing a localized fine search to achieve the best matching of subregions. The flow of a commonly used algorithm is illustrated in Figure 3.
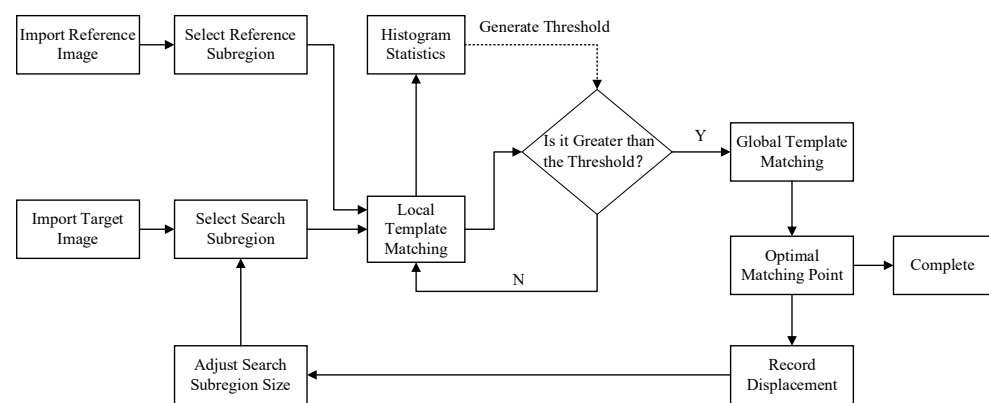

Figure 3   The flow of an algorithm commonly used for integer-pixel search [6]

As engineering demands for precision continue to increase, the physical resolutions of images can no longer meet practical requirements. Therefore, after integer-pixel search, subpixel techniques are employed to increase the accuracy. Typically, by setting the subpixel level to 0.01 pixels, the search precision of DIC is improved to 0.01 pixels. Commonly used subpixel algorithms include grayscale interpolation, inverse compositional methods, surface fitting methods, and the Newton–Raphson partial derivative method [7-9].

3   Measurement Methods

To prevent resonance of the tower caused by impeller rotation, the first- and second-order natural frequencies of the tower must fall within a specified range. However, owing to the large sizes and complex structures of wind turbine towers, measuring their natural frequencies has long been a challenge. The purpose of this test is to measure the natural frequencies and mode shapes of a concrete tower using the DIC method introduced earlier, exploring its application in tower measurement. The test subject is located in Yongzhou, Hunan, China, and was designed and constructed by Huajing Yuda Company in 2023.
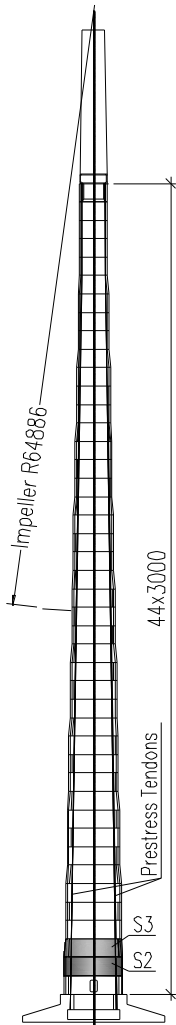
3.1 Design of the Wind Turbine Tower

A common type of wind turbine tower structure is the concrete tower. The concrete tower in this study is assembled from prefabricated concrete tower segments, with the sizes of the prefabricated sections gradually decreasing from bottom to top. Longitudinal external prestressing is applied to provide the system with an integrated ability to resist deformation. The total height of the tower is 160 m, with the concrete tower portion measuring 132 m. It is connected to the wind turbine through a 28 m steel tower segment. The concrete section is divided into 44 segments along its height, with each segment measuring 3 meters in height. Each segment is assembled from three 120° tower panels. The vertical joints between adjacent layers are offset by 60° in the circumferential direction, and the horizontal joints between segments and the vertical joints within segments are filled with epoxy resin. The elevation view of the tower is shown in Figure 4.

3.2 Testing Equipment

The testing equipment consists of a camera and a controller, with a signal acquisition frequency of 40 Hz. It can track the deformation of 70 points simultaneously. A photo of the testing equipment and a working photo are shown in Figure 5.

3.3 Measurement Point Arrangement

One of the key aspects of conducting tests using the DIC method is identifying and marking spots or artificial speckle fields on the tower that can serve as deformation information carriers. As mentioned earlier when describing the basic principles of DIC, the spots serving as information carriers must exhibit a significant color contrast with their surroundings to allow the algorithm to accurately track the pixel positions of the information carriers.

Considering the risks of working at high heights, making new markings on the tower is challenging. In the concrete tower, the vertical joints of two adjacent layers are circumferentially offset by 60°, creating intersection points between the vertical joints and circumferential connection joints. At this point, a significant color contrast with the main body of the tower can be observed and tracked by DIC. Therefore, the intersection between the top of the lower vertical joint and the concrete tower panel of the upper layer is selected as the deformation information carrier, as shown in Figure 6.

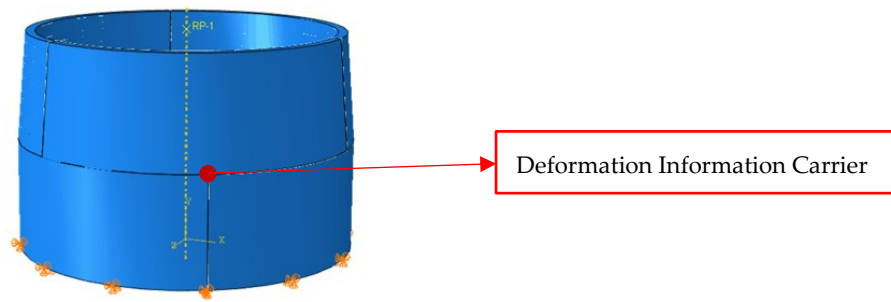**Figure 4** Elevation view of the tower

a) Camera and controller　　　　　　　b) Working photo

Figure 5 Testing Equipment

Figure 6　The deformation information carrier of the tower

Deng et al. reported that for steel towers, four vibration measurement points evenly distributed along the tower's longitudinal direction are sufficient to reconstruct the mode shapes of the entire tower via the modal superposition method [10]. Therefore, a conservative approach of using 8 to 9 measurement points was adopted for this test. The test subjects were wind turbine towers No. 37 and No. 38, both of which have identical turbine and tower structures. The testing distances were 331 m and 447 m from tower No. 37 and tower No. 38, respectively. The measurement point arrangement is shown in Figure 7. For tower No. 37, the distance between measurement points CD_1 and CD_2 is 34 m, with 6 spacing intervals of 18 m each between CD_2 and CD_8 and CD_8 positioned 15 m above the ground. For tower No. 38, the distance between CD_1 and CD_2 is 40 m, with 7 spacing intervals of 15 m each between CD_2 to CD_9 and CD_9 located 15 m above the ground.
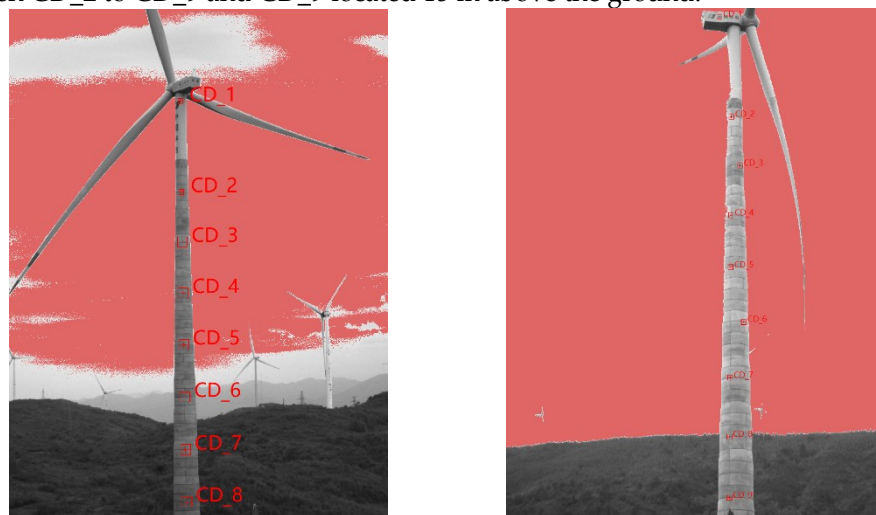
a) Wind turbine tower No. 37 (test distance: 331 m)

b) Wind turbine tower No. 38 (test distance: 447 m)

Figure 7　Measurement point arrangements of the wind turbine towers

3.4　Measurement Procedure

Three conditions were considered in this test to verify the feasibility of applying the DIC method to measure the natural frequencies of concrete towers. Table 1 presents the specific testing conditions.

Table 1　Measurement plan for the natural frequencies of prestressed wind turbine towers

Conditions	Object	Number of measurement points	Measurement distance	Measured mode	Wind turbine status
Condition 1	Tower No. 37	8	331 m	1st fore-aft mode [1] 2nd fore-aft mode	Stoppage

Conditions	Object	Number of measure-ment points	Measurement distance	Measured mode	Wind turbine status
Condition 2	Tower No. 37	8	331 m	1st fore-aft mode / 2nd fore-aft mode	Stable operation
Condition 3	Tower No. 38	9	447 m	1st fore-aft mode / 2nd fore-aft mode	Transition from stoppage to stable operation

[1] The fore-aft mode refers to the vibration mode of the wind turbine tower occurring in the front-to-back direction perpendicular to the plane of the wind blades, which is considered the frontal plane.

The testing procedure is as follows: (a) Secure the tripod and set up the measurement platform, calibrating the measurement distance to ensure that the equipment can monitor the entire wind turbine tower; (b) select measurement points on the basis of the principle that all points should ideally lie along the same straight line, with all points positioned on the side of the wind turbine; (c) calibrate the instruments and adjust the parameters; and (d) operate the wind turbine according to the specified conditions and record the displacement data of the measurement points.

4   Measurement Results

4.1   Data Processing

In the DIC method, noise introduced by the camera system is unavoidable. During the experiments for measuring the natural frequencies of concrete towers, the sources of noise include (a) environmental lighting variations affecting long-distance vibration measurements with DIC; (b) continuous excitation of the structure by wind loads during signal acquisition; and (c) hardware noise from the camera system, primarily due to instability in camera performance, such as speckle noise and dark current noise [11].

4.1.1   High-pass Filter

In this experiment, on the basis of the local meteorological data collected on the test day, the wind load frequency was approximately 0.16 Hz. During turbine operation, the blade rotation rate was approximately 10~12 r/min, corresponding to a periodic excitation frequency of approximately 0.18 Hz acting on the wind tower during the operational phase. To avoid misjudging the natural frequency of the tower in subsequent data analysis, these frequencies can be removed using high-pass filtering. This study employs a Butterworth high-pass filter that is designed to provide a smooth frequency response while achieving sharp signal attenuation at the cutoff frequency. The transfer function of the filter is as follows:

$$H(s) = \frac{(s/\omega_c)^n}{(s/\omega_c)^n + \sum_{k=0}^{n-1} a_k (s/\omega_c)^k + 1} \tag{3}$$

where s is the complex frequency domain variable, ω_c is the cutoff frequency of the filter, n is the order of the filter, and a_k is determined by the pole distribution of the Butterworth high-pass filter. The calculation formula is as follows:

$$\theta_k = \frac{(2k+1)\pi}{2n}, k = 0,1,2,\cdots,n-1 \tag{4}$$

$$s_k = \omega_c(cos(\theta_k) + i \, sin(\theta_k)) \tag{5}$$

$$H(s) = \frac{s^n}{\prod_{k=0}^{n-1}(s - s_k)} \tag{6}$$

where θ_k and s_k represent the angle and the complex value of the poles, respectively. Expanding the denominator of Equation (6) yields a_k. In this experiment, the cutoff frequency is set at 0.2 Hz, and the filter order is 4.

4.1.2 Wavelet Transform

To address potential influencing factors such as variations in environmental lighting and instability in camera performance, this study employs a wavelet transform to reconstruct the signal. This method obtains local time–frequency characteristics by convolving the signal with a mother wavelet. It not only decomposes the low-frequency components of the signal but also captures the transient changes in high-frequency components, making it suitable for processing nonstationary signals [12]. The formula for the wavelet transform is as follows:

$$W_\psi(m,n) = \sum_{k=0}^{N-1} x(t)\psi_{m,n}(t) \tag{7}$$

where m is the scale of the wavelet, n is the position index of the wavelet, $W_\psi(m,n)$ is the transformation coefficient of the vibration data $x(t)$ at scale m and position n, and N denotes the length of the original data. $\psi_{m,n}(t)$ is the mother wavelet function transformed by scale m and position n. In this study, the Daubechies wavelet is used as the mother wavelet.

4.1.3 Calculation of Natural Frequencies and Mode Shapes

The power spectral density of the reconstructed signal is calculated to obtain the natural frequencies of the tower. In this study, the Welch method, with a Hamming window of length 4096, is used. The formula for calculating the power spectral density of the original signal $x[n]$ is as follows:

$$P_{xx}(f) = \frac{1}{M} \sum_{m=0}^{M-1} \frac{1}{U} |X_m(f)|^2 \tag{8}$$

$$U = \frac{1}{N} \sum_{n=0}^{N-1} w^2[n] \tag{9}$$

where $P_{xx}(f)$ is the power spectral density at frequency f, M is the number of segments into which the signal is divided, $X_m(f)$ is the fast Fourier transform (FFT) of the m-th segment of the original signal, U is the energy normalization factor of the window function, N is the length of the window function, and $w[n]$ is the window function. Singular value decomposition (SVD) is subsequently performed to extract the mode shapes of the tower corresponding to the identified frequencies. The data processing workflow is shown in Figure 8.
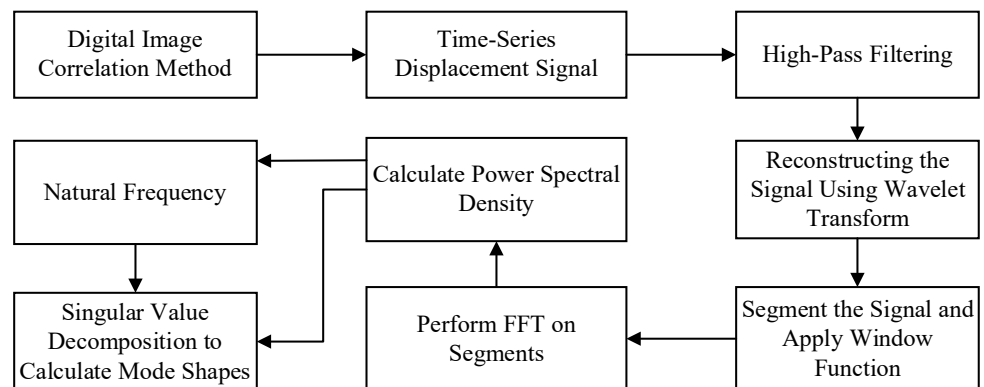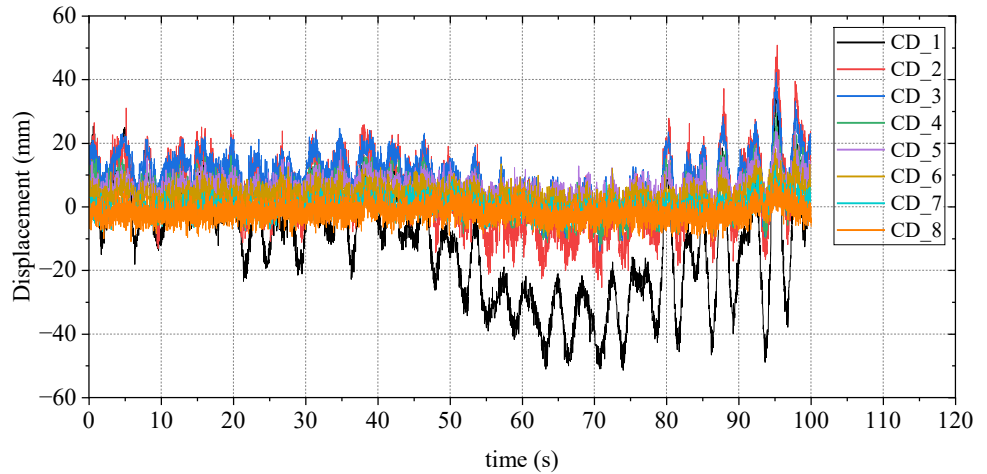

**Figure 8** Schematic diagram of the data processing workflow

4.2 Test Results

4.2.1 Time Series Data

Figures 9 and 10 show the displacement time series data of each measurement point for tower No. 37 during stoppage and stable operation, respectively. The displacement signals were collected over a duration of 100 seconds.
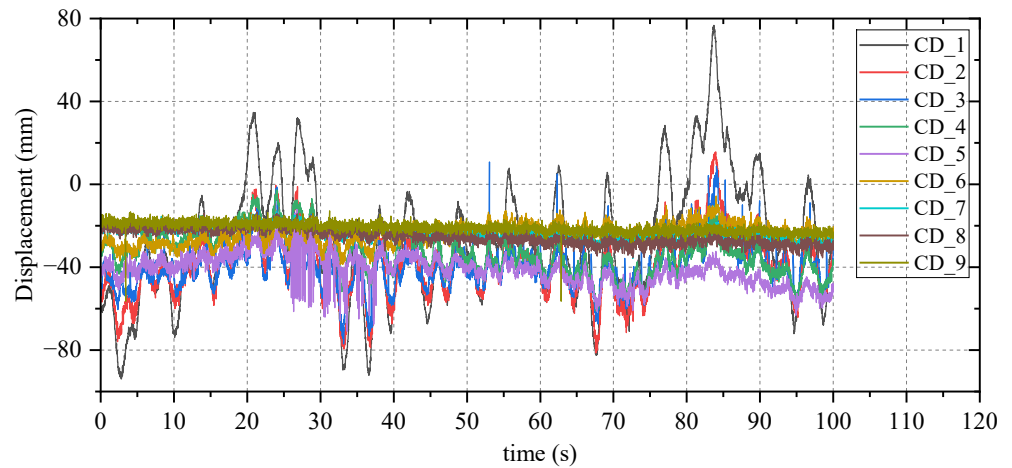

Figure 9 Time series data of each measurement point for wind turbine No. 37 during stoppage
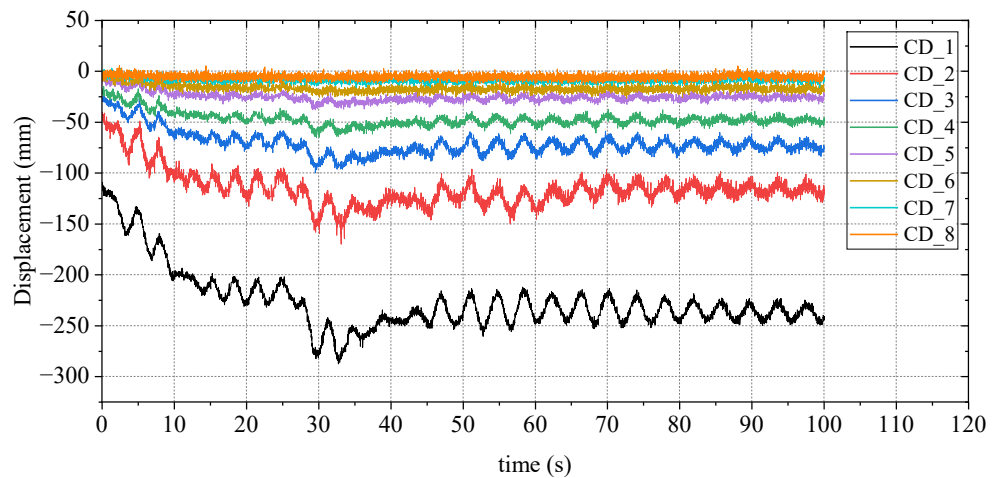
Figure 10 Time series data of each measurement point for wind turbine No. 37 during stable operation

The figures show that during stoppage, the wind turbine is excited by environmental wind, resulting in periodic vibrations centered on zero displacement at each measurement point. The closer the measurement point is to the top of the turbine, the greater the vibration amplitude. During stable operation, the tower is subjected to periodic excitation generated by the turbine's rotation, resulting in forced vibrations. The vibration response at each measurement point is relatively stable, and the displacement increases as the measurement point approaches the top of the turbine.

Figure 11 shows the displacement time series data of each measurement point for wind turbine tower No. 38 during the transition from startup to stable operation. The displacement signals were collected over a duration of 100 seconds.

Figure 11   Time series data of each measurement point for wind turbine No. 38 during the transition from stoppage to stable operation

The figure shows that the vibration responses at the middle-section measurement points CD_4 to CD_6 are greater than those at other points, except for CD_1.

4.2.2   Power Spectral Density

Using the data processing workflow introduced earlier, the power spectral density (PSD) curves for each measurement point of wind turbine tower No. 37 under the two operating conditions were obtained, as shown in Figures 12 and 13.
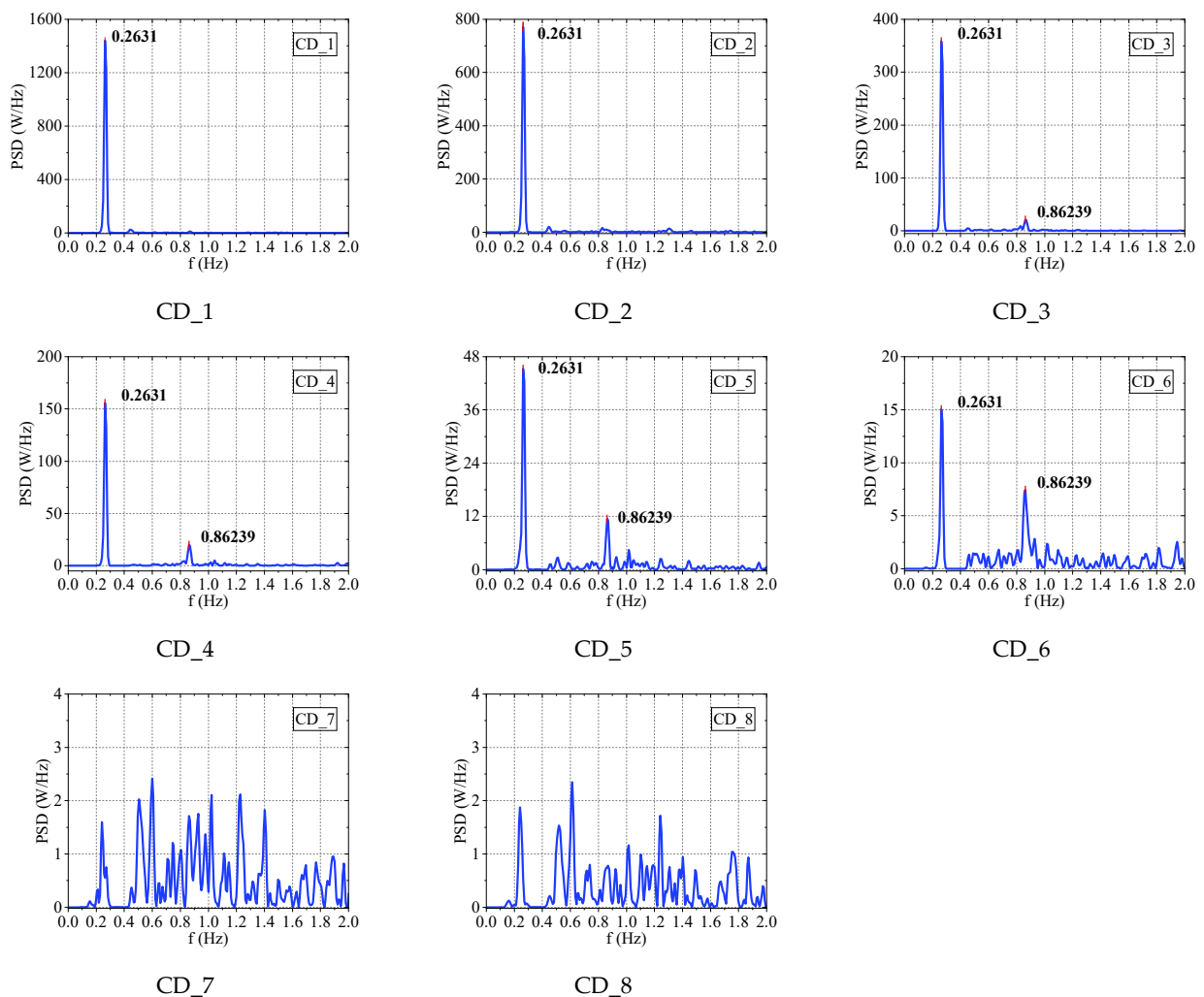
Figure 12   PSD of wind turbine tower No. 37 during stoppage

Figure 12 shows the PSD curves of wind turbine tower No. 37 during stoppage. The figure shows that the first peak of the PSD curves for CD_1 to CD_6 corresponds to a frequency of 0.2631 Hz. Additionally, the PSD at this frequency decreases as the measurement point number increases.

On the basis of the arrangement of measurement points in Figure 7, the following conclusions can be drawn: (a) the higher the measurement point is, the lower the stiffness of its position, resulting in a greater vibration response; (b) it is difficult to identify a second peak on the PSD curves of CD_1 and CD_2, indicating that their vibration response is primarily dominated by the first mode; (c) a distinct second peak can be observed in each of the PSD curves of CD_3 to CD_6, with a frequency of 0.8624 Hz; and (d) the PSDs at all frequencies for measurement points CD_7 and CD_8 are relatively small, making it difficult to identify a distinct peak. This is because their positions have greater structural stiffness, resulting in weak vibration responses under environmental wind excitation.

In summary, the first natural frequency of wind turbine tower No. 37 under these conditions is 0.2631 Hz, and the second natural frequency is 0.8624 Hz.

Figure 13 shows the PSD curves of wind turbine tower No. 37 during stable operation. The first peak of each of the PSD curves for measurement points CD_1 to CD_6 corresponds to a frequency of 0.2636 Hz. For measurement points CD_1 and CD_2, a second peak close to the first peak is observed, with a frequency of 0.30 Hz. The second peaks for measurement points CD_3 to CD_5 are all at 1.0397 Hz. The PSD curve of CD_6 does not have a distinguishable second peak, and the PSDs of CD_7 and CD_8 at all frequencies are relatively small, making it difficult to identify clear peaks.
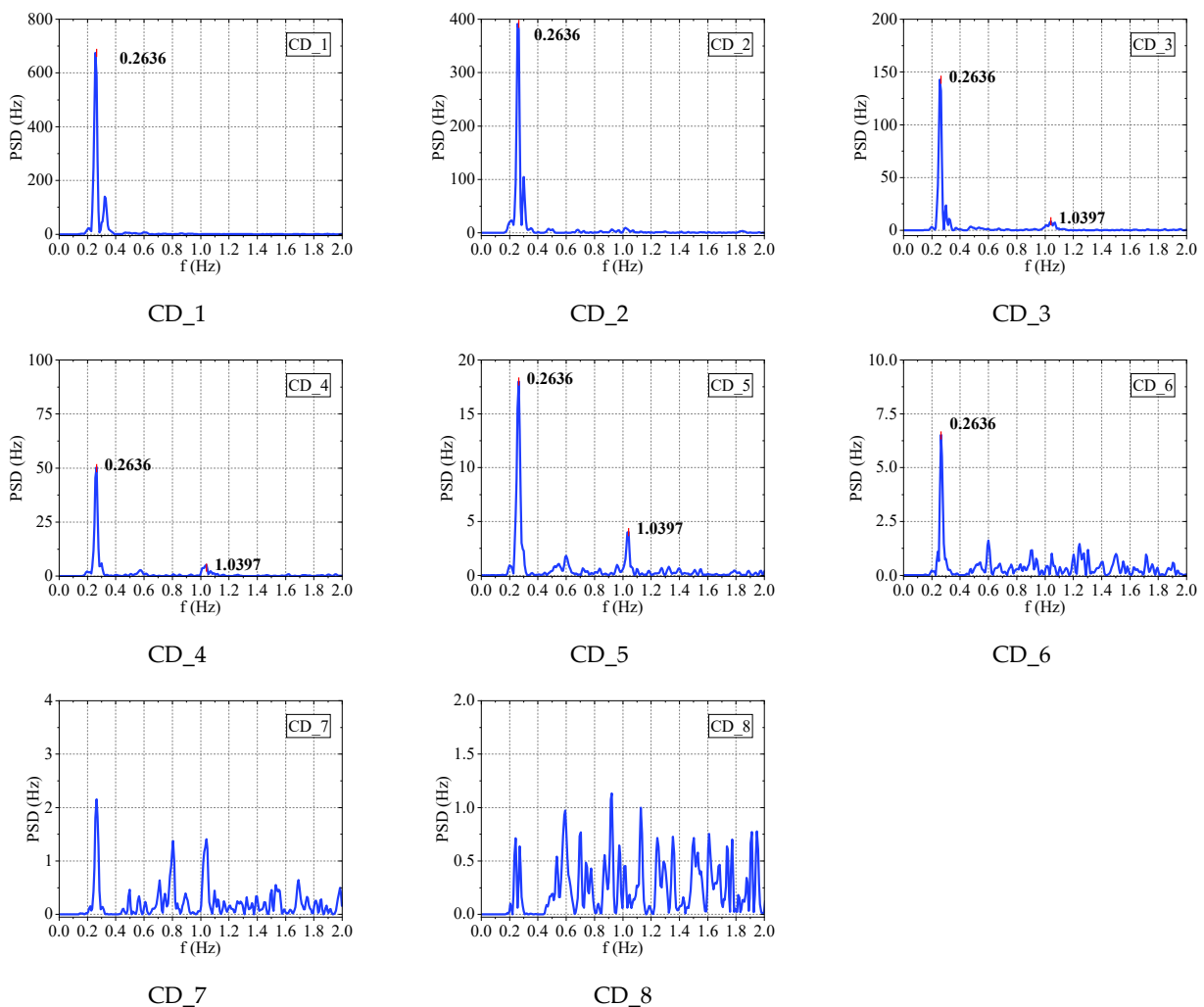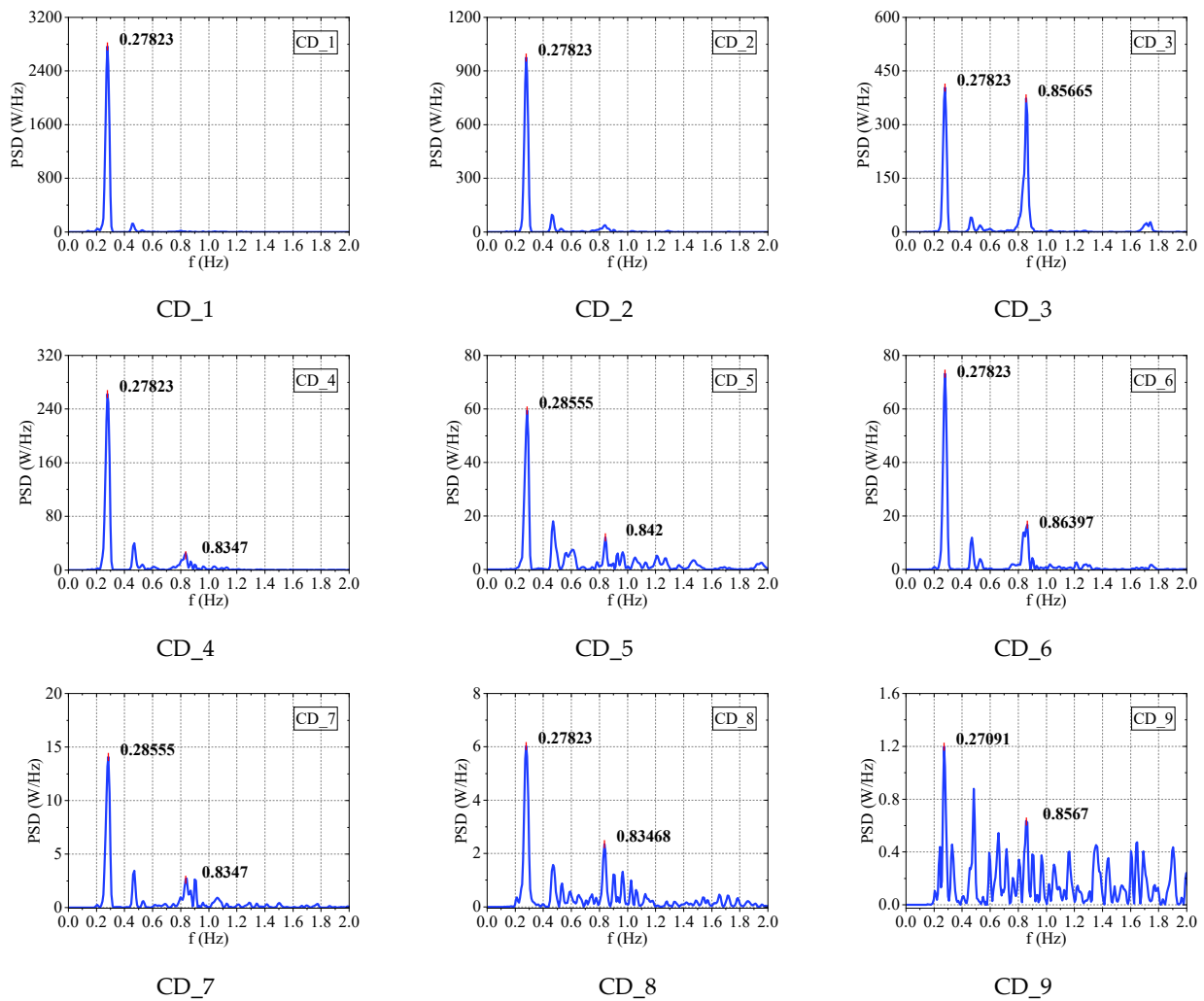

Figure 13   PSD curves of wind turbine tower No. 37 during stable operation

In summary, under these conditions, the first natural frequency of wind turbine No. 37 is measured as 0.2636 Hz. The second natural frequency is difficult to measure under these conditions but is estimated to be 1.0397 Hz.

Figure 14 shows the power spectral density curves of each measurement point for wind turbine No. 38 during the time period from startup to stable operation.

Figure 14 shows that the first peak for all the measurement points has a frequency of approximately 0.2782 Hz. Like in the case of tower No. 37, the energy of measurement point CD_1 and that of measurement point CD_2 are concentrated at the frequency of the first peak. The second peak frequencies of the PSD curves for measurement points CD_3, CD_4, CD_5, andCD_6 are 0.8566 Hz, 0.8347 Hz, 0.8420 Hz, and 0.8640 Hz, respectively. Additionally, each of the PSD curves for measurement points CD_7 to CD_9 also show a peak near 0.84 Hz. The inconsistency in peak frequencies across measurement points may be due to unavoidable disturbances caused by the continuously changing rotational speed of the turbine at the tower top under these operating conditions. Considering that the peak frequencies across all the measurement points are very close, their mode is taken as the natural frequency. Thus, the first natural frequency of tower No. 38 is 0.2782 Hz, and the second natural frequency is 0.8374 Hz.

Figure 14　PSD curves of wind turbine tower No. 38 during the transition from stoppage to stable operation

Table 2 compares the first and second natural frequencies of towers No. 37 and No. 38 under different operating conditions.

Table 2 Natural frequencies of wind towers under different conditions

| Conditions	Object	First natural frequency (Hz)	Second natural frequency (Hz)	Wind turbine status
Condition 1	Tower No. 37	0.2631	0.8624	Stoppage
Condition 2	Tower No. 37	0.2636	1.0397	Stable operation
Condition 3	Tower No. 38	0.2782	0.8374	Transition from stoppage to stable operation

The table shows that the first natural frequencies under the three conditions are relatively close, whereas the second natural frequencies under Conditions 1 and 3 are also similar. However, the second natural frequency measured under Condition 2 differs significantly from those measured under the other two conditions, likely because of the stable rotation of the wind blades exciting a hidden mode at that frequency. Therefore, when the DIC method is used to measure the natural frequencies of prestressed concrete towers, the influence of blade rotation on the tests should be minimized.

4.2.3 Mode Shapes

The natural frequencies obtained from the PSD curves can be used to derive the first- and second-order mode shapes of wind turbine tower No. 37 using the SVD method. Figure 15 shows the first- and second-order mode shapes measured during the stoppage of tower No. 37, whereas Figure 16 presents the first- and second-order mode shapes measured during stable operation. Figure 17 shows the first- and second-order mode shapes of wind turbine tower No. 38 measured during the transition from stoppage to stable operation.
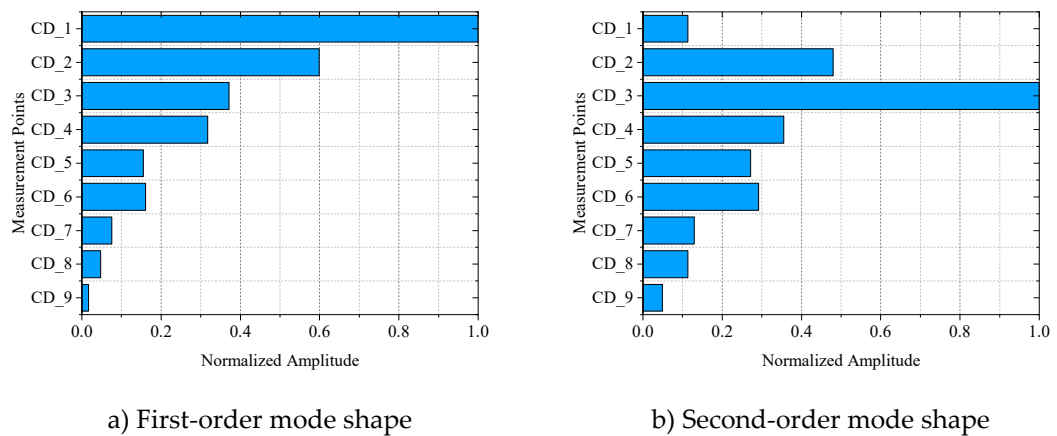

a) First-order mode shape   b) Second-order mode shape
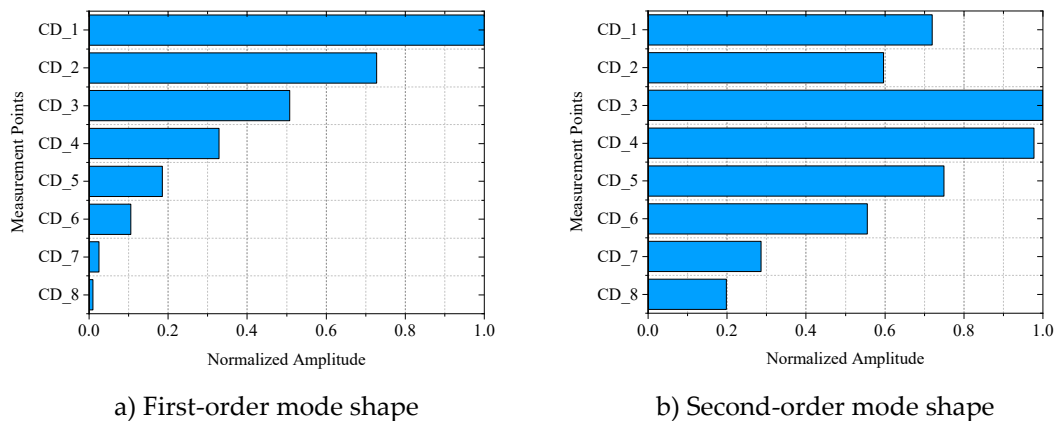
Figure 15 Mode shapes of wind turbine tower No. 37 during stoppage

a) First-order mode shape   b) Second-order mode shape
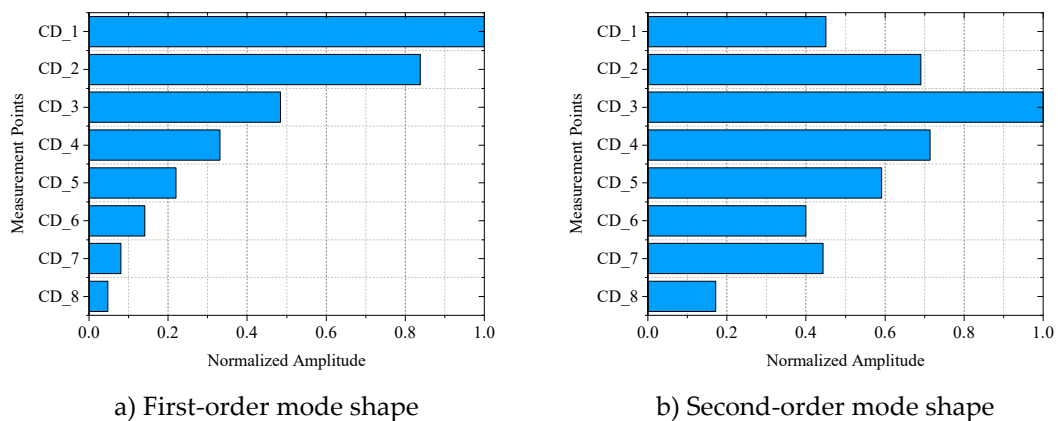
Figure 16 Mode shapes of wind turbine tower No. 37 during stable operation

The figures show that under the first-order mode shape, the tower exhibits uniform bending in a single direction, with the entire structure assuming a bent configuration. In contrast, the second-order mode shape displays reverse bending, where the middle section of the tower bends in one direction, whereas the top and bottom sections bend in the opposite direction.

The first-order mode shapes measured under the two conditions are relatively consistent. However, differences are observed in the second-order mode shape at CD_1, where the vibration amplitude at this point during turbine operation is smaller than that during turbine stoppage. This may be because the rotation plane of the wind blades is perpendicular to the bending vibration plane being measured. During blade rotation, the rotational inertia increases the effective stiffness in the bending direction because of the inertia in the direction perpendicular to the bending plane. Consequently, this reduces the vibration response at higher points on the tower. The increased stiffness results in the natural frequencies measured during turbine operation being higher than those measured during turbine stoppage.

a) First-order mode shape   b) Second-order mode shape

Figure 17   Mode shapes of wind turbine tower No. 38 during the transition from stoppage to stable operation.

A comparison of Figures 15, 16 and 17 reveals that the first-order mode shapes measured under the three conditions all exhibit unidirectional bending, whereas the second-order mode shapes display reverse bending. The main difference lies in the reduced actual vibration response of the tower top measurement point (CD_1) during blade rotation. Moreover, from the pattern in Figure 11, where the displacement amplitudes of each measurement point tend to be larger in the middle and smaller at both ends, it can be inferred that the second-order vibration mode constitutes a significant proportion of the vibration response of the wind tower during the transition from stoppage to stable operation.

5   Conclusions

This paper introduces the basic principles of and algorithmic steps for applying the DIC method to measure the natural frequencies of wind towers. The natural frequencies and mode shapes of structurally identical wind turbine towers No. 37 and No. 38 were measured. The main conclusions are as follows:

(1)   Applying the DIC method to measure the natural frequencies of concrete towers effectively avoids the potential safety risks and implementation difficulties associated with the traditional approach of installing sensors on the tower body. This method is fast, convenient, and has been validated by numerous studies.

(2)   When the turbine is stopped, the first and second natural frequencies of the wind tower measured using the DIC method are 0.2631 Hz and 0.8624 Hz,

respectively. During stable operation, the measured first and second natural frequencies are 0.2636 Hz and 1.0397 Hz, respectively. During the transition from stoppage to stable operation, the measured first and second natural frequencies are 0.2782 Hz and 0.8374 Hz, respectively.

(3) The mode shapes measured under the three conditions are relatively similar. During turbine operation, the rotational inertia of the wind blades weakens the vibration response at measurement points located at higher positions on the tower.

(4) There are slight differences in the measurement results under the three conditions, primarily due to the operational state of the turbine. Therefore, when the DIC method is used for measurement, to minimize measurement errors, the turbine should not be in operation.

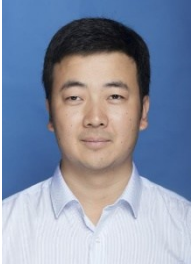**Conflict of Interest**: All authors disclosed no relevant relationships.

Data Availability Statement: The data that support the findings of this study are available from the corresponding author, Wei, upon reasonable request.

References

1. China Agricultural Machinery Industry Association Wind Power Machinery Branch. China Wind Power Industry Development Report (2023). *Electric Age* **2023**, 14-19.

2. Yang, C.; Cui, H.; Zhang, Z. Calculation of Inherent Frequency of Wind Turbine Tower. *Energy and Conservation* **2023**, 6-9,37, doi:10.3969/j.issn.2095-0802.2023.01.002.

3. Lei, Z.; Liu, G.; Yang, W.; Li, Y. Analytical Calculation Method for the Pre-stress Basic Frequency of Wind Turbine Towers Based on Rayleigh Method. *Journal of Vibration and Shock* **2022**, *41*, 23-29,65, doi:10.13465/j.cnki.jvs.2022.10.004.

4. Yang, C.; Wang, R.; Zhang, J. Numerical Method for Calculating System Fundamental Frequencies of Offshore Wind Turbines with Monopile Foundations. *Engineering Mechanics* **2018**, *35*, 219-225, doi:10.6052/j.issn.1000-4750.2017.01.0046.

5. Pan, B.; Qian, K.M.; Xie, H.M.; Asundi, A. Two-Dimensional Digital Image Correlation for In-plane Displacement and Strain Measurement: A Review. *Measurement Science and Technology* **2009**, *20*, 1-17, doi:10.1088/0957-0233/20/6/062001.

6. Xu, Y.; Gao, Z.; Hu, P. Application of Whole-Pixel Search Algorithms to Optical Measurements. *Mechanical and Electrical Information* **2019**, 113-115, doi:10.3969/j.issn.1671-0797.2019.18.057.

7. Li, S.; Gao, X.; Liu, Z.; Hu, W. Algorithm for Sub-Pixel Detection of Fringe Image Displacement Based on Gray-Level Interpolation. *Acta Optica Sinica* **2021**, *41*, 125-133, doi:10.3788/aos202141.1012002.

8. Meng, X.; Xu, Q.; Xiao, S.; Li, Y.; Zhao, B.; Li, G. Performance of Sub-Pixel Displacement Iterative Algorithm Based on Digital Image Correlation Method. *Acta Optica Sinica* **2024**, *44*, 129-146, doi:10.3788/aos231480.

9. Li, K.; Cai, P. Study on the Performance of Sub-pixel Algorithm for Digital Image Correlation. *Chinese Journal of Scientific Instrument* **2020**, *41*, 180-187, doi:10.19650/j.cnki.cjsi.J2006554.

10. Deng, M.; Deng, A.; Zhu, J.; Xu, Q.; Wang, S.; Wang, S. Research on Real-Time State of Wind Turbine Tower Based on Modal Superposition Method. *Acta Energiae Solaris Sinica* **2021**, *42*, 63-70, doi:10.19912/j.0254-0096.tynxb.2018-1091.

11. Li, Y.; Si, G.; Guo, Y. Noise Analyzing and Processing for Scientific Grade CCD Camera. *Optics and Precision Engineering* **2005**, *13*, 158-163, doi:10.3321/j.issn:1004-924X.2005.z1.032.

12. Leng, J.; Diao, K.; Pang, Z.; Feng, H. Automatic Identification Method of Modal Parameters of Offshore Platform Structure Based on IEWT. *Journal of Vibration and Shock* **2024**, *43*, 196-204, doi:10.13465/j.cnki.jvs.2024.07.021.

AUTHOR BIOGRAPHIES

Zhenwei Guo D.Eng, Studying at Civil Engineering, Tongji University. Research Direction: Modified concrete materials, Bridge Engineering. Email: 2410030@tongji.edu.cn	**Kangle Chen** D.Eng, Working at Shanghai Zhengruida Renewable Energy Co., Ltd. Research Direction: Structural Design and Optimization of Wind Turbine Tower. Email: chenkangle@zwindtowers.com
Zhongze Sun M.Eng, Working at Dongfang Electric Wind Power Co., Ltd. Research Direction: Structural Design and Optimization of Wind Turbine Tower.	**Lei Hong** B.E., Working at Wuhan Sinorock Monitor & Control Technology Co., Ltd. Research Direction: Digital Image Correlation Technology. Email: honglei@whrsm.com
Yan Xu B.E., Engineer, Working at Tongna Testing & Certification Group Co., Ltd. Research Direction: Engineering Construction Monitoring Email: 675388727@qq.com	**Sihang Wei** D.Eng, Working at Shanghai Zhengruida Renewable Energy Co., Ltd. Research Direction: Structural Design and Optimization of Wind Turbine Tower. Email: weisihang@zwindtowers.com